Cement and Concrete Research 42 (2012) 673–685

Contents lists available at SciVerse ScienceDirect

Cement and Concrete Research

journal homepage: http://ees.elsevier.com/CEMCON/default.asp

Microstructural and compositional change of NaOH-activated high calcium fly ash by incorporating Na-aluminate and co-existence of geopolymeric gel and C–S–H(I)

Jae Eun Oh [a,b], Juhyuk Moon [a], Sang-Gyun Oh [c], Simon M. Clark [d,e], Paulo J.M. Monteiro [a,*]

[a] Department of Civil and Environmental Engineering, University of California, Berkeley, CA 94720, USA
[b] School of Urban and Environmental Engineering, Ulsan National Institute of Science and Technology, Ulsan Metropolitan City, 689-798, South Korea
[c] Department of Architectural Engineering, Dong-Eui University, 995 Eomgwangro, Busanjin-Gu, Busan 614-714, South Korea
[d] Advanced Light Source, Lawrence Berkeley National Laboratory, Berkeley, CA 20015, USA
[e] Department of Earth and Planetary Sciences, Macquarie University, Sydney, NSW 2109, Australia

ARTICLE INFO

Article history:
Received 28 July 2011
Accepted 7 February 2012

Keywords:
C–S–H (B)
X-ray diffraction (B)
Fly ash (D)
Alkali activated cement (D)
Geopolymer

ABSTRACT

This study explores the reaction products of alkali-activated Class C fly ash-based aluminosilicate samples by means of high-resolution synchrotron X-ray diffraction (HSXRD), scanning electron microscope (SEM), and compressive strength tests to investigate how the readily available aluminum affects the reaction. Class C fly ash-based aluminosilicate raw materials were prepared by incorporating Na-aluminate into the original fly ashes, then alkali-activated by 10 M NaOH solution. Incorporating Na-aluminate reduced the compressive strength of samples, with the reduction magnitude relatively constant regardless of length of curing period. The HSXRD provides evidence of the co-existence of C–S–H with geopolymeric gels and strongly suggests that the C–S–H formed in the current system is C–S–H(I). The back-scattered electron images suggest that the C–S–H(I) phase exists as small grains in a finely intermixed form with geopolymeric gels. Despite providing extra source of aluminum, adding Na-aluminate to the mixes did not decrease the Si/Al ratio of the geopolymeric gel.

1. Introduction

Despite cement and concrete industries now using a large portion of fly ash as admixtures, a sizable amount of fly ash continues to be disposed into landfill. In 2004, the United States generated 70.8 million tons of coal fly ash and 42.7 million tons of this ash was disposed into ground or ocean [1]. In 2007, Europe (EU 15) produced 41 million tons of coal fly ash, but the re-utilization rate was only 47% [2]. Because fly ashes contain quite high level of leachable toxic trace elements (such as As, Cd, Cu, Hg, Ni, Pb, B and Zn, etc.), the excess fly ash that is not being recycled may contaminate the soil, ocean, and water reservoir, presenting a severe threat to human health and ecosystems [3]. The recycling of fly ash is now one of the top environmental and economical issues. Geopolymer production using recycled coal fly ash as a main source material is one promising solution [4]. Not only have geopolymers been shown to potentially replace Portland cement in concrete production (as they have comparable mechanical properties, much lower CO_2 production, and cost) [5], but they also have an excellent ability to immobilize hazardous heavy elements, dissolved in contaminated soils, by locking the heavy elements in a three-dimensional geopolymer network structure [5].

Class C fly ash (FAC) (known as high-calcium fly ash) is an industrial waste by-product produced by burning lignite and subbituminous coals, and contains at least more than 20% of CaO. Class F fly ash (FAF) (known as low-calcium fly ash) is produced by burning anthracite and bituminous coals, and contains little CaO. The chemical composition of FAC is somewhere between that of ground granulated blast furnace slag (GGBFS)–which arises from rapid cooling of molten blast furnace slag in iron manufacture–and FAF with respect to its major chemical components: CaO, Al_2O_3, and SiO_2. Therefore, it is assumed that the reaction products of alkali-activated FAC may share some features found in alkali-activated FAF and alkali-activated GGBFS [6], opening up the intriguing possibility of exploiting similar known characteristics, such as the coexistence of C–S–H and geopolymeric gel. The key to understanding the compositional characteristics of alkali-activated FAC is the role of Ca in the fly ash. To date, most geopolymer studies using fly ash have focused on FAF, with much less discussion regarding alkali-activation of FAC and the role of Ca [7–11].

The role of Ca as an additive for little-to-none Ca-containing aluminosilicate materials (e.g., metakaolin or FAF) has been extensively studied [9–16]. The possible additive Ca sources have been GGBFS, Portland cement, and chemicals such as $Ca(OH)_2$ or calcium silicates (e.g., C_3S), etc., in the expectation that adding Ca will form co-existing C–S–H with the geopolymeric gel. No definite evidence exists, such as convincing X-ray diffraction reflections for C–S–H phase; only semi-quantitative (or qualitative) chemical analysis data of SEM or poor quality of X-ray diffraction patterns is available [12,14–16]. These results are further complicated by the fact that the electron beam size for the chemical probe is likely to be much

* Corresponding author.
E-mail address: monteiro@berkeley.edu (P.J.M. Monteiro).

0008-8846/$ – see front matter © 2012 Elsevier Ltd. All rights reserved.
doi:10.1016/j.cemconres.2012.02.002

larger than the sizes of the homogeneous phases [e.g., grains of C–S–H, geopolymer, $Ca(OH)_2$, or unreacted raw materials] found in matrices; therefore, the chemical analysis results often show the compositional average of different phases. For studies of C–S–H and geopolymeric gel, it is very important to locate the homogeneous areas that are large enough to contain only a single phase; otherwise, the measurements of the chemical data using SEM are not reliable.

Earlier studies have demonstrated that the atomic Si/Al ratio of geopolymer matrices, forming generally in the range of 1–4 [5], largely affects mechanical properties (e.g., compressive strength and Young's modulus); therefore, the optimum ratio of Si/Al for the highest strength appears at near 2 [17]. Note that, however, this observation was made from metakaolin-based geopolymer studies. Since metakaolin is mainly a pure and reactive glassy material (i.e., most Si and Al react and form geopolymer), the Si/Al ratio of geopolymer is very close to that of the raw metakaolin; however, this may not be valid for Class C fly ash, because various complex reactions (e.g., C–S–H and geopolymer co-formation) exist and also the amounts of reactive phases are smaller. For instance, considerable amount of Si or Al may be present in less reactive constituents such as mullite or quartz. This makes it difficult to predict how the addition of Al-sources will affect the Si/Al ratio of the geopolymer reaction products. In principle, modifications of the Si/Al ratio by adding an extra source of aluminum could be an efficient way to adjust the mechanical properties of Class C fly ash-based geopolymer products; however, little research has been done on the influence of additive Na-aluminates on alkali-activation of Class C fly ash [18].

The present study explores the reaction products of alkali-activation of FAC-based aluminosilicate system by 10 M NaOH solution by means of high-resolution synchrotron X-ray diffraction (HSXRD), SEM, and compressive strength tests. The first goal of this study is to show the co-existence of C–S–H(I) and geopolymeric gel in NaOH based alkali-activated FAC system, and, second, to explore the influence of Na-aluminates on the microstructure and mechanical properties of activated Class C fly ash samples.

2. Experimental

Two Class C fly ashes (labeled as FAC1 and FAC2) were obtained for this study. In addition, two mixtures of the original fly ashes with Na-aluminate (labeled as Na-FAC1 and Na-FAC2) were prepared to create test samples containing high concentrations of Ca with varying atomic Si/Al ratios. The chemical composition of the raw materials–determined by X-ray fluorescence (XRF)–is given in Table 1. These raw materials were alkali-activated with analytical grade 10 M NaOH solution (Fisher Scientific, Certified ACS pellets) and cured at 80 °C with 100% relative humidity for the entire curing period (up to 32 days). The solution to solid binder weight ratio (s/b) of samples used for compressive strength tests and SEM analysis was set to 0.4. The HSXRD samples were synthesized with s/b = 1.33. The reason for using a great amount of solution was to maximize the crystallinity of the alkali-activated samples because poor crystallinity of alkali-activated aluminosilicate samples creates difficulties in analyzing the X-ray diffraction data [7,14,15]. One day curing for the HSXRD samples was enough to achieve high crystallinity in X-ray diffractograms. A major difference between the SEM samples and the HSXRD samples was mostly the amount of activator solution (i.e., s/b) while the other significant conditions such as raw materials, NaOH solution concentration, curing temperature and curing humidity were the same. Details of the mixture proportions of the samples are presented in Table 2.

Table 1
Chemical composition of raw materials used for activated samples.

Major elements as oxide (wt.%)	Raw materials and mixtures used for below samples			
	FAC 1 group		FAC 2 group	
	FAC1	Na-FAC1	FAC2	Na-FAC2
SiO_2	40.19	33.2	27.69	24.92
TiO_2	1.22	1.01	1.33	1.2
Al_2O_3	18.69	26.26	17.32	21.81
Fe_2O_3	5.15	4.25	5.62	5.06
K_2O	0.72	0.59	0.35	0.31
MnO	0.01	0.01	0.02	0.01
CaO	20.6	17.02	30.28	27.25
MgO	5.69	4.7	8.39	7.55
Na_2O	3.4	9.39	3.24	6.7
P_2O_5	–	–	–	–
SO_3	1.01	0.83	2.32	2.09
LOI	3.33	2.75	3.45	3.11
Al_2O_3/SiO_2 (wt./wt.)	0.47	0.79	0.63	0.88
Si/Al (atomic ratio)	1.82	1.07	1.36	0.97
Ca/Si (atomic ratio)	0.55	0.55	1.17	1.17
Ca/Mg (atomic ratio)	2.6	2.6	2.59	2.59

Note that FAC1, FAC2, Na-FAC1 and Na-FAC2 are the names of the activated samples.

Table 2
Mixture proportions of activated samples (wt.%).

Sample label	Original raw materials			NaOH solution (10 M)	s/b (wt./wt.)	Curing temp. (°C)
	FAC1	FAC2	Na-aluminate			
FAC1	71.4	0.0	0.0	28.6	0.40	80.0
Na-FAC1	58.9	0.0	12.5	28.6	0.40	
FAC2	0.0	71.4	0.0	28.6	0.40	
Na-FAC2	0.0	64.3	7.1	28.6	0.40	

Note: s/b = solution to solid binder weight ratio; for HSXRD test, the amount of NaOH solution was increased to make s/b = 1.33.

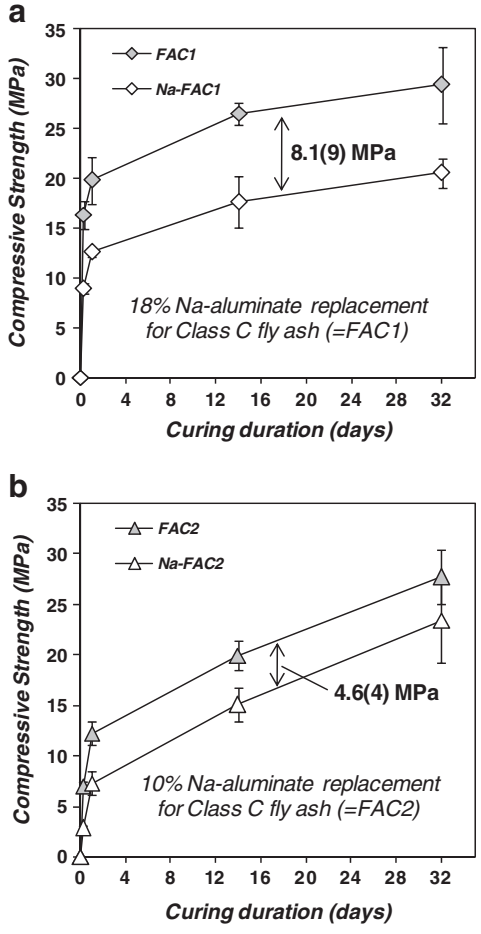

Fig. 1. Strength development of alkali-activated fly ash based aluminosilicate samples (10 M NaOH, s/b = 0.4 at 80 °C).

The samples for the compressive strength tests were cast in cylindrical molds measuring ϕ2.54 cm × 2.54 cm using the same conditions to the SEM samples with varying curing periods. The samples were cured for 6 h, 1 day, 7 days, 14 days, and 32 days (at 80 °C with 100% relative humidity), with the test results averaged (using three activated cylinders for each mixture after curing) using a Baldwin Universal testing machine. The HSXRD samples were air-dried and ground into fine powder for the HSXRD tests. The diffraction patterns were collected at beamline 12.2.2 at the Advanced Light Source, Lawrence Berkeley National Laboratory, using a wavelength of λ = 0.4959 Å. Peak positions were identified by fitting the HSXRD data with pseudo-Voigt profiles using the XFIT program. The SEM images for the chemical analysis were collected using ZEISS EVO®MA10. Hardened cylindrical samples were cut in half and cured for 14 days. For each sample, one side was polished and carbon-coated for the chemical analysis (SEM-EDS) and back scattered images (BSE), and the other paired side of the sectioned sample was gold-coated without polishing for high-resolution secondary electron image (SE).

3. Results and discussion

Compressive strength development of all alkali-activated samples is summarized in Fig. 1. The immediate availability of high aluminum concentration was expected to promote the formation of geopolymeric gel and to increase the compressive strength; however, incorporating Na-aluminate resulted in a decrease in compressive strength, proportional to the amount of the added Na-aluminate. The reason for this decrease requires further study. Note that the magnitude of strength reduction remained relatively constant [8.1(9) MPa for Na-FAC1 and 4.6(4) MPa for Na-FAC2] in each sample regardless of the length of curing period. The FAC1 sample gained strength much quicker than FAC2, but the strengths of both samples were similar after curing for 32 days.

The HSXRD patterns were collected after curing for one day at 80 °C under dilute condition of s/b = 1.33 (see Fig. 2). Note some new diffraction peaks formed during the alkali-activation. The *d*-spacings of the new peaks are tabulated in Table 3 with the phases identified by labels. In all samples, C–S–H(I) phase [with characteristic peaks of C–S–H(I) at *d* = 12.5, 3.07, and 2.82 Å (see Table 3)] manifested itself as a main reaction product, together with the geopolymeric gel which is observed as an amorphous hump around 2.0–4.0 Å [7–9,15,16]. It is not surprising that hydroxycancrinite and basic sodalite phases were found in all samples as they are structurally related to the geopolymeric gel formed in high concentration NaOH activation of fly ash (they share a 6-membered aluminosilicate ring, the same basic building unit) [7]. Note that the addition of Na-aluminate resulted in a decrease of the intensity of C–S–H(I) peaks, and an increase in the crystalline hydroxycancrinite and basic sodalite signals (see Fig. 2), which might explain the decrease in compressive strength for Na-FAC1 and Na-FAC2 samples.

The pattern profile of C–S–H(I) formed in the current study is very close to that of an alkali-activated GGBFS (see Fig. 2) [7], strongly suggesting that C–S–H(I) products are almost identical in their structure. This requires further study of the C–S–H(I) formed in alkali-activated GGBFS system [17,19,20] to understand the C–S–H(I) of the current alkali-activated FAC-based aluminosilicates. The HSXRD pattern for the activated Na-FAC2 sample was quite different from those of the other samples, which are similar to one another. In Na-FAC2 sample,

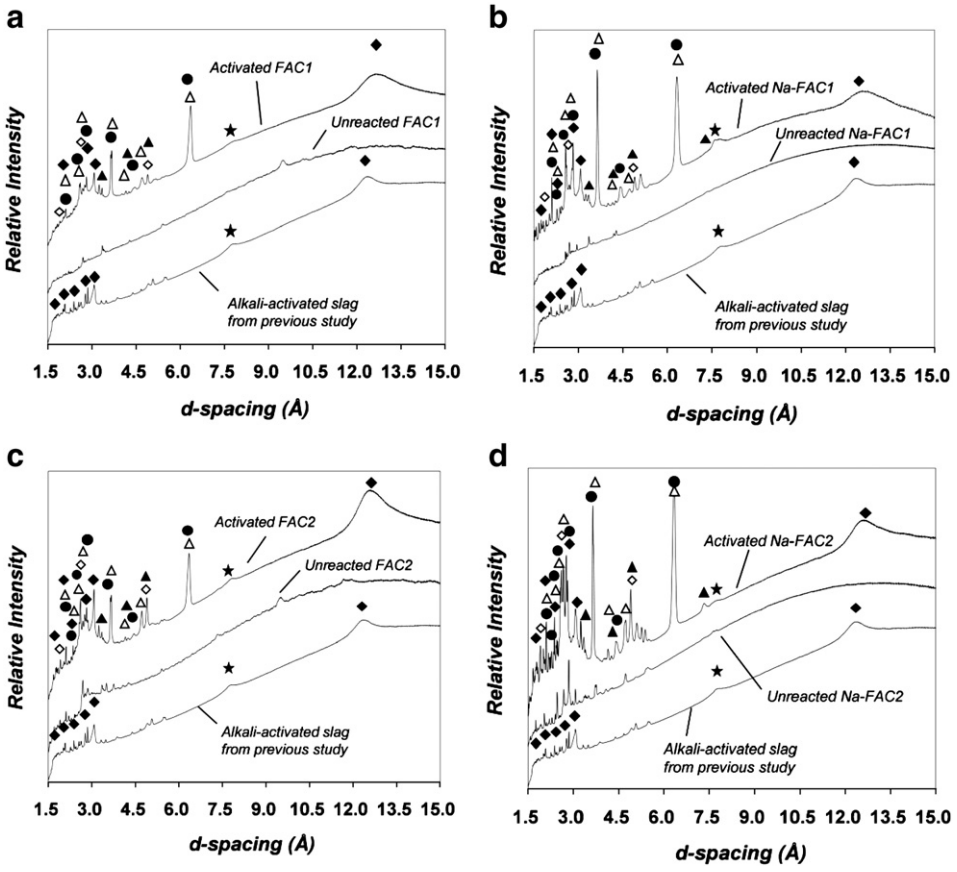

Fig. 2. High resolution X-ray diffractograms of powder samples made by alkaline activation of dilute FAC-based aluminosilicate samples (s/b = 1.33), cured for 24 h at 80 °C with 100% relative humidity; s/b = solution to binder weight ratio. The symbols indicate: ● = basic sodalite (hydrated form of hydroxysodalite), △ = hydroxycancrinite, ♦ = C–S–H(I), ★ = hydrotalcite-like phase, ◊ = portlandite and ▲ = gismondine. Activated samples are designated with 'activated' and raw materials are shown with 'unreacted' in the figures. The HSXRD pattern for alkali-activated GGBFS is taken from previous study (s/b = 0.4, cured for 6 h at 80 °C with 100% relative humidity) [7]. The chemical composition of GGBFS is presented in Ref. [7].

Table 3
Identified newly formed XRD reflections in HSXRD samples.

d-spacings (Å)					Identified phase (typical d-spacings in Å in the literature)
FAC1	Na-FAC1	FAC2	Na-FAC2	Activated GGBFS [7]	
12.57	12.57	12.53	12.52	12.50	C–S–H(I) (12.5)
7.80	7.76	7.80	7.73	7.77	Hydrotalcite-like (7.64–7.844)
–	–	–	7.33	–	Gismondine (7.28)
6.36	6.35	6.36	6.35	–	Hydroxycancrinite (6.43)
6.31	6.31	6.30	6.30	–	Basic sodalite (6.28)
5.50	5.50	5.50	5.50	–	
–	–	–	5.37	–	
–	–	5.26	5.26	–	
5.09	5.10	5.10	5.10	5.08	
4.89	4.89	4.90	4.91	4.93	$Ca(OH)_2$ (4.90)/ gismondine (4.91)
4.73	4.74	4.73	4.73	–	Hydroxycancrinite (4.70)
4.69	4.69	4.69	4.69	–	
–	–	–	–	4.66	
4.45	4.44	4.45	4.45	–	Basic sodalite (4.44)
4.40	4.40	4.39	4.40	4.40	
4.26	4.26	4.26	4.26	–	Gismondine (4.27)
–	–	4.23	4.23	4.23	
4.16	4.15	4.15	4.16	–	Hydroxycancrinite (4.17)
4.15	–	4.13	4.13	–	
4.02	4.02	4.02	4.02	–	
3.98	3.99	3.99	3.98	–	
–	–	–	–	3.85	Hydrotalcite-like (3.88)/ calcite (3.852)
–	–	–	–	3.71	
3.67	3.67	3.67	3.67	–	Hydroxycancrinite (3.68)
3.64	3.64	3.64	3.64	–	Basic sodalite (3.63)
–	–	–	–	3.54	
–	–	3.39	3.39	–	
3.34	3.34	3.34	3.34	–	Gismondine (3.34)
–	3.32	–	3.32	3.33	
3.25	3.25	3.24	3.25	–	
–	–	–	–	3.19	
–	3.14	–	3.14	–	
–	3.10	–	3.11	–	
3.07	3.07	3.07	3.07	3.07	C–S–H(I) (3.07)
3.00	3.00	3.00	2.99	–	
–	–	2.86	–	–	
2.82	2.82	2.82	2.82	2.79	C–S–H(I) (2.80)/ hydroxysodalite (2.81)
2.77	2.78	2.77	2.77	2.77	
–	–	–	–	2.74	
–	–	–	–	2.66	
–	–	2.63	2.63	2.63	
2.60	2.60	2.60	2.61	2.59	$Ca(OH)_2$ (2.628)/ hydrotalcite-like (2.566–2.608)
2.57	2.57	2.57	2.57	–	Basic sodalite (2.56)
2.54	2.54	2.54	2.54	2.54	
–	–	–	2.45	–	
2.37	2.38	2.38	2.38	–	Hydroxysodalite (2.37)
–	–	2.35	2.35	–	
–	–	2.28	2.28	2.27	Hydrotalcite-like (2.28–2.33)/calcite (2.284)
2.12	2.12	2.12	2.12	–	Hydroxycancrinite (2.122)
2.10	2.10	2.10	2.10	–	Basic sodalite (2.090)/calcite (2.094)
–	2.07	–	2.07	2.06	
–	2.02	–	2.01	2.02	
1.91	1.91	1.92	1.92	1.93	$Ca(OH)_2$ (1.927)
1.84	1.83	1.84	1.83	1.83	C–S–H(I) (1.83)
1.79	1.79	1.78	1.79	1.80	Ca(OH)2 (1.796)
–	–	–	–	1.73	
–	–	–	–	1.69	
1.67	1.67	1.67	1.67	1.66	C–S–H(I) (1.67)

C–S–H(I) phase is identified according to JCPDS 34-0002 and 06-0010; hydrotalcite-like phase is identified according to JCPDS 14-0191, 22-0700, 41-1428 and [19]; hydroxycancrinite is identified according to JCPDS 46-1457; basic sodalite is identified using JCPDS 11-0401 for hydroxysodalite; gismondine is identified according to JCPDS 39-1373 and 20-0452; and $Ca(OH)_2$ (=portlandite) is identified according to JCPDS 04–0733.

the major crystalline phases were still C–S–H(I), hydroxycancrinite, and basic sodalite, but relatively strong peaks of gismondine were also formed together with unknown extra peaks.

The earlier study by Oh et al. [7] found much weaker C–S–H(I) diffraction peaks in similar alkali-activated FAC system. Although the sample was synthesized from the same method, it was made of a different Class C fly ash source with a CaO content of 19.9%. This sample showed lower compressive strength, probably due to less C–S–H(I) formation compared to the samples in this present study. Thus, C–S–H(I) formation is not governed solely by the high Ca content of raw fly ash, but possibly related to reactivity of Ca [7], which may vary depending on the source of the Class C fly ash.

High-resolution SEM secondary electron (SE) images are presented in Fig. 3 through Fig. 6. Matrices containing Na-aluminate (i.e., Na-FAC1 and Na-FAC2) are clearly more homogeneous, with fewer crystalline products. Crystalline products were mainly found in pore areas of FAC1 and FAC2 samples. Platy-shaped crystals [see Fig. 3(c)] were visible in the pore areas of FAC1. The crystals in Fig. 5(c) may be basic sodalite (or hydroxysodalite); the crystals in Fig. 5(d) most likely are unreacted mullite crystals. The matrices with Na-aluminate appeared to have much less amount of these crystals, but the matrices were not compact either, which might explain the decrease in compressive strength in the SEM SE images [compare Figs. 3(a), 4(a), 5(a), and 6(a)].

The elemental spot analysis and BSE images are presented in Fig. 7 through Fig. 10 and Table 4 through Table 8, implying the formation of geopolymers and C–S–H(I) in the alkali-activated samples. Note that the electron beam size of SEM-EDS spot analysis (~1 μm in diameter) was larger than the sizes of most grains of geopolymer or C–S–H(I); therefore, locating large single-phase blocks in the sample matrices was critical for an accurate analysis of the chemical composition of the samples.

The Si/Al atomic ratios of geopolymer reaction products decreased compared to the original Si/Al ratios of raw materials in FAC1 (1.82 for the original ash; 0.8 for the geopolymer) and FAC2 (1.36 for original ash; 1.0 for geopolymer) samples; the Si/Al ratios for the Na-FAC1 and Na-FAC2 samples remained almost the same from the raw materials. This implies that (1) the initial ratio of Si/Al in raw fly ashes cannot be used as a practical indicator of predicting the ratio of Si/Al in FAC-based geopolymer products, which is in contrast to geopolymers made of metakaolin [6], because a portion of Si and Al are possessed by less reactive minerals (e.g., mullite) or some reactive Si and Al may be involved in C–S–H(I) or Al-substituted C–S–H(I) formation; (2) the addition of Na-aluminate (i.e., extra Al source) tends to increase (or at least maintain) the Si/Al of geopolymer products (e.g., Si/Al = 0.8 for FAC1 geopolymer; Si/Al = 1.04 for Na-FAC1 geopolymer), and increase the atomic ratio of (Na + K)/Al, as found in an earlier study (see Figs. 11 and 12) [18,21].

Theoretically, the ratio of alkaline metal ions to aluminum in geopolymeric gel should be near one to compensate a charge deficiency in the geopolymer structure [5]; however, several researchers have reported that there is a large variance in the (Na + K)/Al ratio geopolymer matrices [5,18,21]. In addition, the compressive strength usually increases proportional to the Si/Al ratio up to two in the geopolymeric gel. The optimum Si/Al ratio for maximum compressive strength has been reported to be near two [5,18]. Interestingly in this study, Si/Al ratios of geopolymeric gels showing the highest compressive strength had the lowest Si/Al (=0.8) and (Na + K)/Al (=0.6). Thus, because of the high chemical complexity of fly ash, these two compositional factors [i.e., Si/Al and (Na + K)/Al in the geopolymer] may not be indicative of the compressive strength in the case of an alkali-activated FAC system.

In the BSE images, phases consisting of mainly heavier elements are "brighter", thus similar compositional phases can be identified, using this "brightness" as a benchmark. Thus, geopolymeric products can be identified in matrices where the same level of "brightness" is

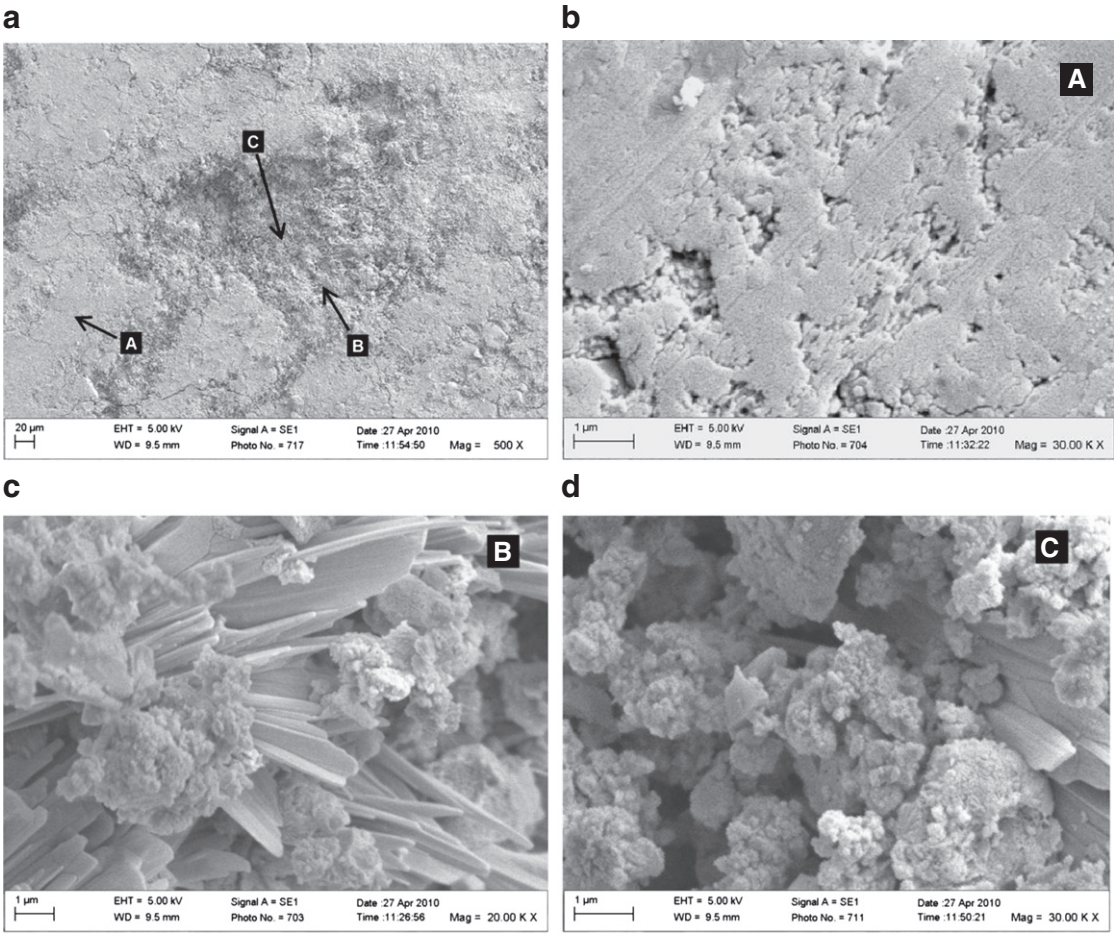

Fig. 3. Microstructure of activated FAC1 sample observed by SEM SE image mode; (b) is the area of A; (c) is the area of B; and (d) is the area of C in (a).

evident (see Fig. 7 through Fig. 10). Obviously, the geopolymer phases, appearing as particulate products in the polished sample surfaces, are seen as dark gray grains and indicated by white and black arrows in a magnified BSE image shown in Fig. 13(a) (note that it is a magnified figure of the section Z in Fig. 10). This conclusion is confirmed by the chemical composition of position M1 in Fig. 13(a) and (c), presenting a typical chemical composition as found in the geopolymers of this current study. Note that these particulate grains show similar brightness to the identified geopolymer blocks seen in Fig. 7 through Fig. 10. The SE image in Fig. 13(b) suggests a possible corresponding morphology of the particulate geopolymer products (see black arrows). A similar morphology of geopolymer particulate grains were observed in BSE and SE images for all samples (see Fig. 14). The incorporation of Na-aluminate results in an increase in these particulate grain sizes [compare grain sizes in Fig. 14(a) and (b)].

In the alkali-activation of aluminosilicate materials containing Ca–particularly for cases of alkali-activation of GGBFS and metakaolin blends–SEM BSE images of C–S–H phases have been observed in a segregated form from geopolymeric gels [14–16]. In the current study, however, a segregated C–S–H phase was not observed in the BSE images, similarly in [20], except for a single case (see Fig. 8), which was a large separate area showing a chemical composition similar to that of C–S–H(I) [Ca/Si = 0.74(4) and Al/Si = 0.3(2)] [20]. Considering the strong evidence of C–S–H(I) formation shown in the HSXRD patterns, it is concluded that C–S–H(I) products form with sizes in the range of approximately hundreds of nanometer and up to 1 µm and intermix with the geopolymers when FAC-based aluminosilicate materials are alkali-activated. This explanation is qualitatively supported by the chemical spot analysis shown in Fig. 15. The chemical composition of position M1 [= possibly mixed area of C–S–H(I) and the geopolymer] can be constructed as a combination of chemical compositions of position C1 [= possibly C–S–H(I)] and position 1 (= a possible geopolymer) by appropriate scaling and overlapping of spot analysis diagrams; note that the approximate chemical composition of position M1 = 0.71 × position 1 + 0.29 × position C1. In addition, SEM-EDS spot analysis indicates that nearly all the small bright grains (hundreds nanometer to ~1 µm), which are shown as white spots in all BSE images, contain considerable Ca with Mg, which is possibly related to C–S–H(I) [17,19,20]. It was not possible to isolate the chemical composition of the white grains because the sizes of particles were too small compared to the electron beam size (~1 µm in diameter). A similar conclusion for C–S–H formation was drawn in an earlier study for alkali-activated GGBFS-FAF blending mixture [22], where the authors concluded that the discrete sizes of C–S–H phases that formed separately from the geopolymer were due to inadequate mixing of raw materials of GGBFS and FAF.

4. Conclusions

Compressive strength of samples decreased with increasing amounts of Na-aluminate. The reduction magnitude of strength was kept relatively constant [8.1(9) MPa for Na-FAC1 and 4.6(4) MPa for Na-FAC2], regardless of length of curing period. High-resolution SEM(SE) images and SEM-EDS show that incorporating Na-aluminate into original Class C fly ash results in: (1) growth in the grain size of the geopolymer grain size; (2) increase in Si/Al ratio in Class C fly ash geopolymer products, in spite of adding aluminum,

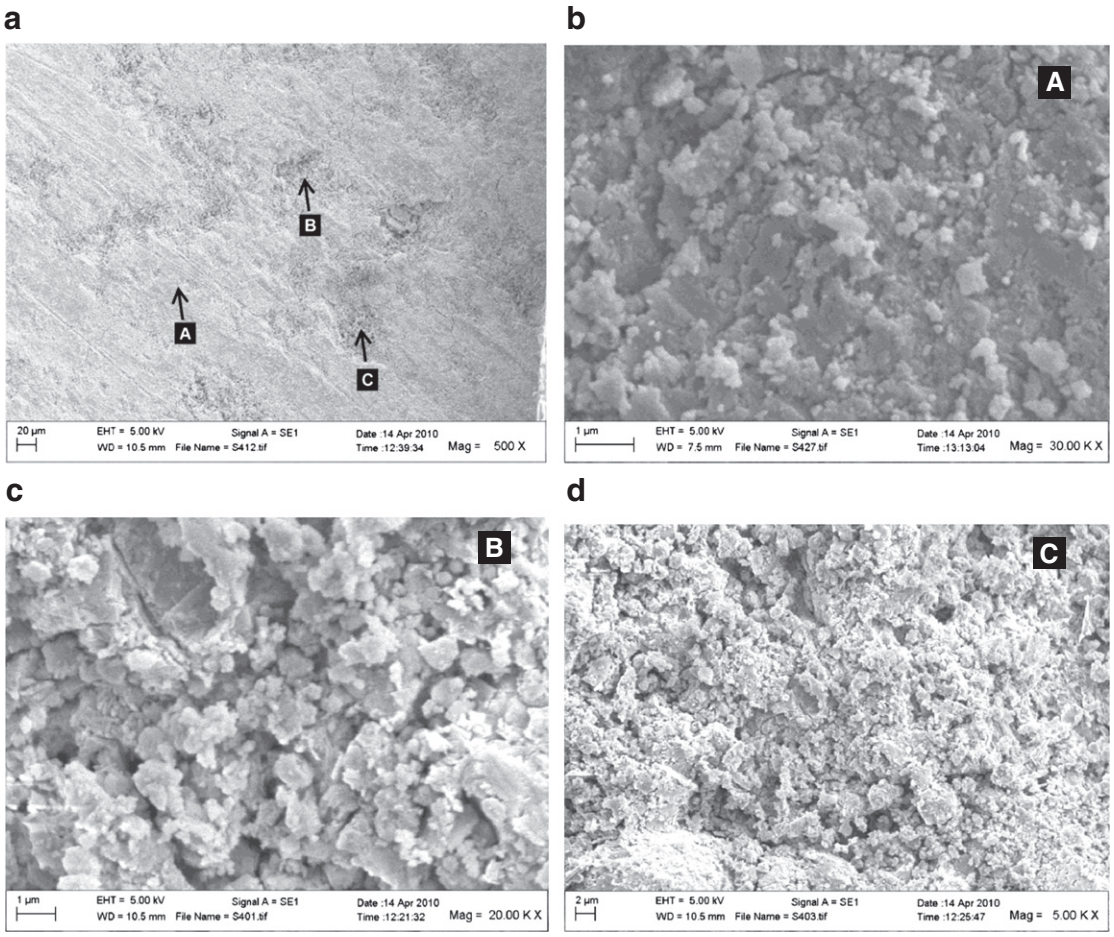

Fig. 4. Microstructure of activated Na-FAC1 sample observed by SEM SE image mode; (b) is the area of A; (c) is the area of B; and (d) is the area of C.

resulting in a Si/Al ratio of near one; (3) significant decrease in crystals in activated matrices; and (4) more homogeneous but less dense activated matrices. High-resolution synchrotron X-ray diffraction diagrams provide strong evidence of co-existence of C–S–H(I) with geopolymeric gels in alkali-activated FAC-based aluminosilicate system as the diffraction pattern profile of the C–S–H (I) phase in the current study is very similar to that of alkali-activated GGBFS. Although segregated geopolymer phases were easily observed in all samples, a discrete macro-size of C–S–H(I) block was difficult to be seen from the SEM BSE images, strongly suggesting that the C–S–H(I) phase exists in fine grain sizes (less than ~1 μm) in an intermixed form with geopolymeric gels.

Acknowledgments

This publication was based on the work supported in part by Award no. KUS-l1-004021, made by King Abdullah University of Science and Technology (KAUST) and by NIST Grant no. 60NANB10D014. The Advanced Light Source is supported by the Director, Office of Science, Office of Basic Energy Sciences, of the U.S. Department of Energy under Contract no. DE-AC02-05CH11231.

References

[1] American Coal Ash Association (ACAA), website:, http://www.acaa-usa.org/.
[2] European Coal Combustion Products Association (ECOBA), Website:, http://www.ecoba.com/.
[3] S. Sharma, M.H. Fulekar, C.P. Jayalakshmi, C.P. Straub, Fly ash dynamics in soil–water systems, Crit. Rev. Environ. Sci. Technol. 19 (1989) 251–275.
[4] M. Ahmaruzzaman, A review on the utilization of fly ash, Prog. Energy Combust. Sci. 36 (2010) 327–363.
[5] D. Khale, R. Chaudhary, Mechanism of geopolymerization and factors influencing its development: a review, J. Mater. Sci. 42 (2007) 729–746.
[6] P. Duxon, J.L. Provis, Designing precursors for geopolymer cements, J. Am. Ceram. Soc. 91 (2008) 3864–3869.
[7] J.E. Oh, P.J.M. Monteiro, S.S. Jun, S. Choi, S.M. Clark, The evolution of strength and crystalline phases for alkali-activated ground blast furnace slag and fly ash-based geopolymers, Cem. Concr. Res. 40 (2010) 189–196.
[8] X. Guo, H. Shi, W.A. Dick, Compressive strength and microstructural characteristics of class C fly ash geopolymer, Cem. Concr. Compos. 32 (2010) 142–147.
[9] X. Guo, H. Shi, L. Chen, W.A. Dick, Alkali-activated complex binders from class C fly ash and Ca-containing admixtures, J. Hazard. Mater. 173 (2010) 480–486.
[10] I. Garcia-Lodeiro, A. Palomo, A. Fernandez-Jimenez, D.E. Macphee, Compatibility studies between N–A–S–H and C–A–S–H gels. Study in the ternary diagram Na_2O–CaO–Al_2O_3–SiO_2–H_2O, Cem. Concr. Res. 41 (2011) 923–931.
[11] E.M. Gartner, D.E. Macphee, A physico-chemical basis for novel cementitious binders, Cem. Concr. Res. 41 (2011) 736–749.
[12] J. Temuujin, A. Van Riessen, R. Williams, Influence of calcium compounds on the mechanical properties of fly ash geopolymer pastes, J. Hazard. Mater. 167 (2009) 82–88.
[13] J. Van Deventer, J. Provis, P. Duxson, G. Lukey, Reaction mechanisms in the geopolymeric conversion of inorganic waste to useful products, J. Hazard. Mater. 139 (2007) 506–513.
[14] C. Yip, J. Van Deventer, Microanalysis of calcium silicate hydrate gel formed within a geopolymeric binder, J. Mater. Sci. 38 (2003) 3851–3860.
[15] C. Yip, G. Lukey, J.S.J. van Deventer, The coexistence of geopolymeric gel and calcium silicate hydrate at the early stage of alkaline activation, Cem. Concr. Res. 35 (2005) 1688–1697.
[16] C.K. Yip, G.C. Lukey, J.L. Provis, J.S.J. van Deventer, Effect of calcium silicate sources on geopolymerisation, Cem. Concr. Res. 38 (2008) 554–564.
[17] P. Duxson, J.L. Provis, G.C. Lukey, S.W. Mallicoat, W.M. Kriven, J.S.J. van Deventer, Understanding the relationship between geopolymer composition, microstructure and mechanical properties, Colloids Surf., A 269 (2005) 47–58.
[18] J. Phair, J.S.J. van Deventer, Characterization of fly-ash-based geopolymeric binders activated with sodium aluminate, Ind. Eng. Chem. Res. 41 (2002) 4242–4251.

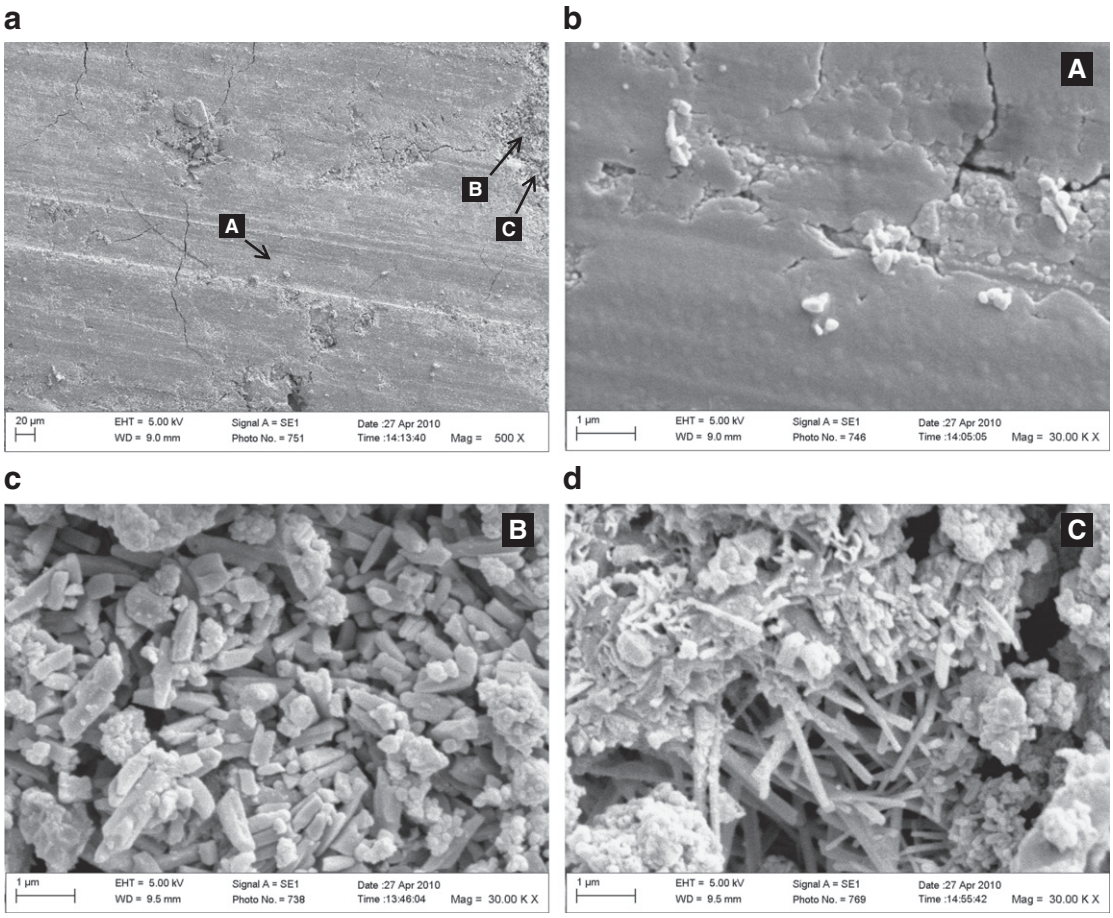

Fig. 5. Microstructure of activated FAC2 sample observed by SEM SE image mode; (b) is the area of A; (c) is the area of B; and (d) is the area of C.

[19] S.D. Wang, K.L. Scrivener, Hydration products of alkali activated slag cement, Cem. Concr. Res. 25 (1995) 561–571.
[20] I. Richardson, A. Brough, G. Groves, C. Dobson, The characterization of hardened alkali-activated blast-furnace slag pastes and the nature of the calcium silicate hydrate (CSH) phase, Cem. Concr. Res. 24 (1994) 813–829.
[21] A. Palomo, M.W. Grutzeck, M.T. Blanco, Alkali-activated fly ashes: a cement for the future, Cem. Concr. Res. 29 (1999) 1323–1329.
[22] R.R. Lloyd, J.L. Provis, J.S.J. van Deventer, Microscopy and microanalysis of inorganic polymer cements. 2: The gel binder, J. Mater. Sci. 44 (2009) 620–631.

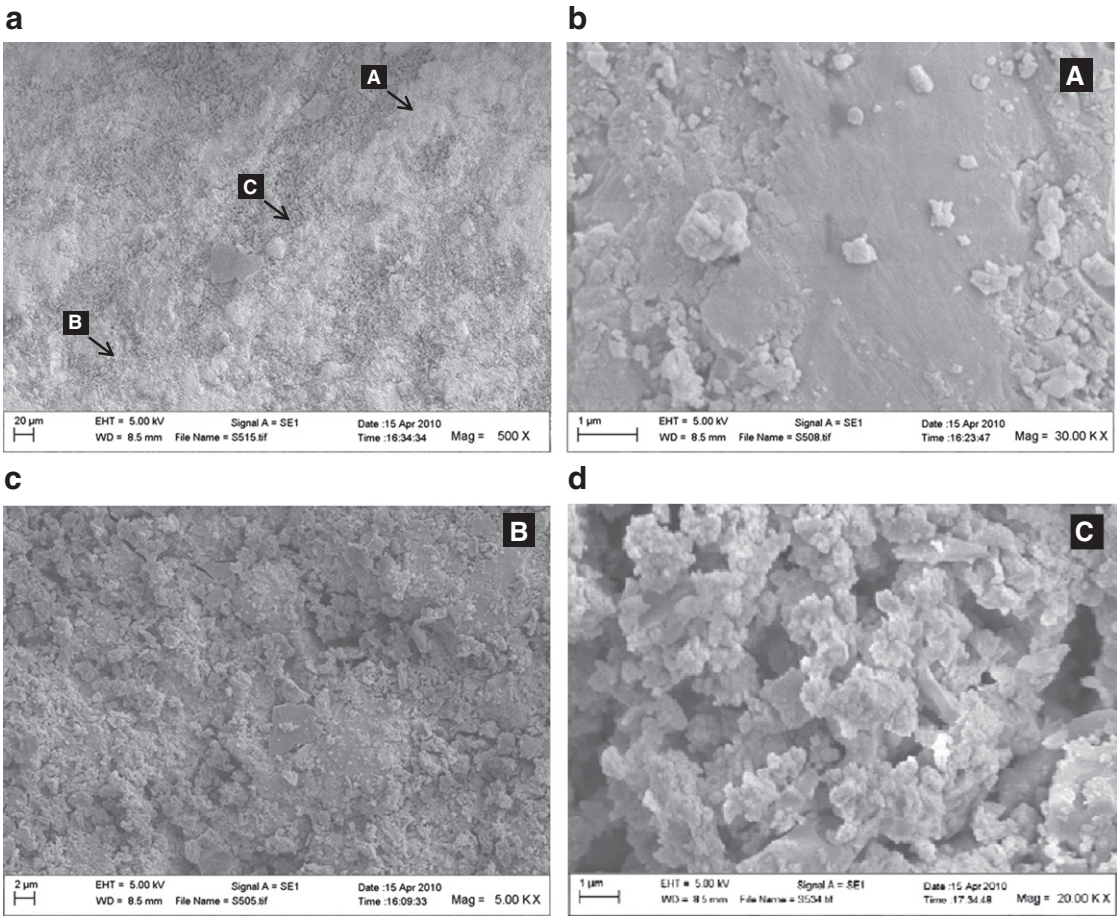

Fig. 6. Microstructure of activated Na-FAC2 sample observed by SEM SE image mode; (b) is the area of A; (c) is the area of B; and (d) is the area of C.

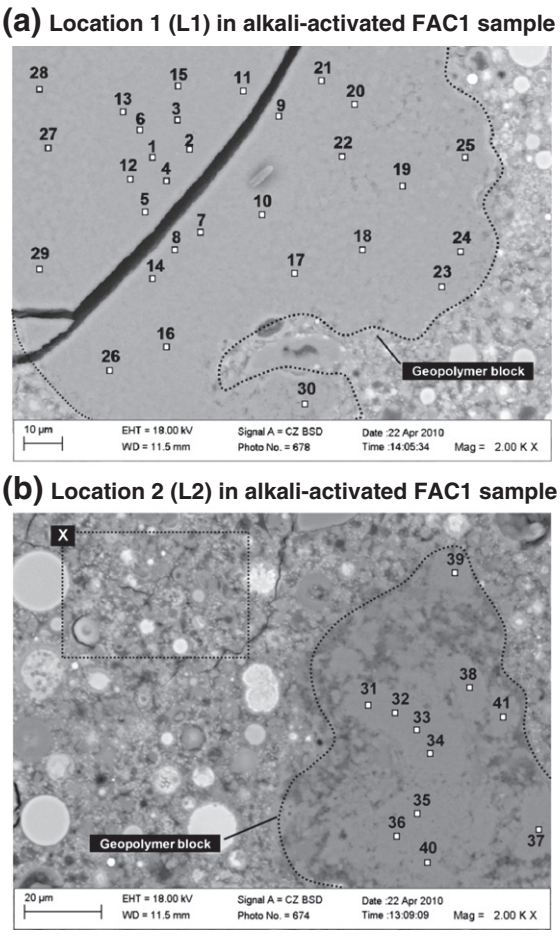

Fig. 7. Backscattered SEM images of carbon-coated polished section for two different locations in activated FAC1 sample with no addition of Na-aluminate.

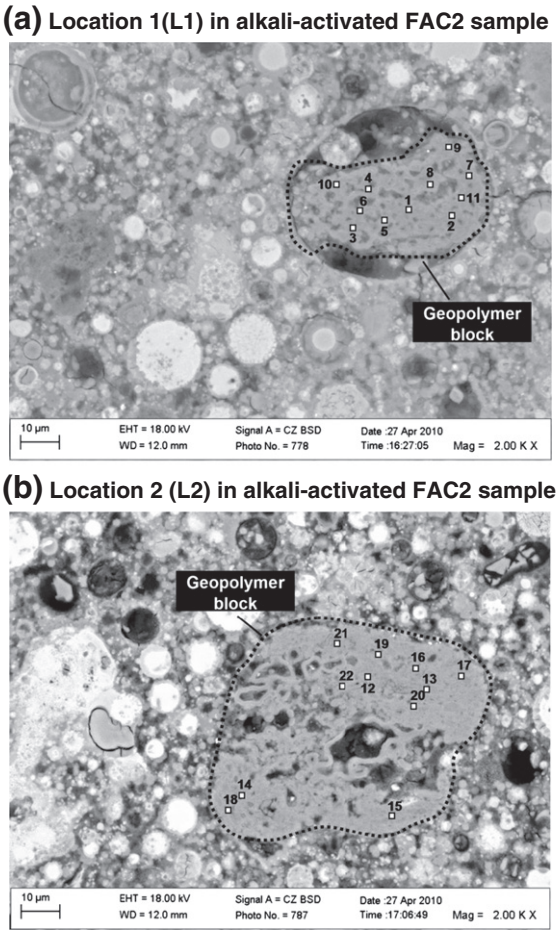

Fig. 9. Backscattered SEM images for alkali-activated FAC2 sample (no Na-aluminates added).

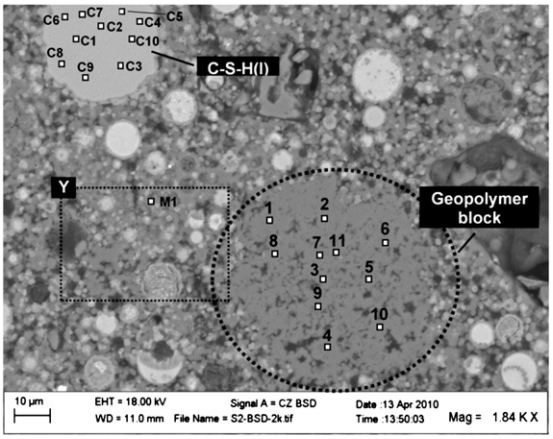

Fig. 8. Backscattered SEM image for alkali-activated Na-FAC1 sample (Na-aluminates added).

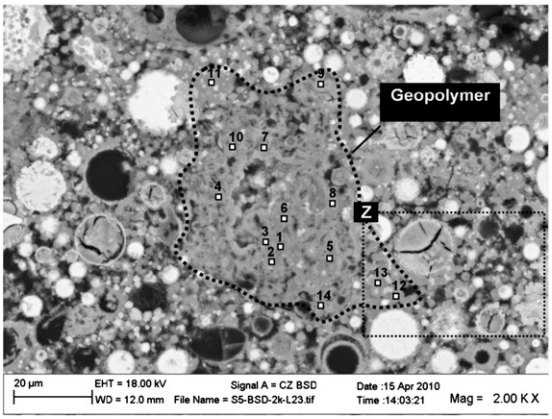

Fig. 10. Backscattered SEM image for alkali-activated Na-FAC2 sample (Na-aluminates added).

Table 4
Chemical compositions (at.%) of geopolymer phase in alkali-activated FAC1 of Fig. 7.

Location	Positions	Na	Mg	Al	Si	K	Ca	Fe	Si/Al	(K + Na)/Al
L1	1	8.30	0.24	12.10	9.30	0.18	0.16	0.00	0.77	0.70
	2	6.23	0.23	9.68	7.33	0.27	0.15	0.00	0.76	0.67
	3	7.40	0.20	11.26	8.55	0.30	0.11	0.00	0.76	0.68
	4	5.45	0.12	11.23	8.42	0.26	0.18	0.00	0.75	0.51
	5	6.67	0.25	11.49	8.83	0.35	0.12	0.00	0.77	0.61
	6	7.05	0.21	11.76	9.21	0.30	0.12	0.00	0.78	0.63
	7	5.92	0.30	9.80	7.03	0.17	0.13	0.00	0.72	0.62
	8	6.49	0.39	11.04	8.16	0.36	0.11	0.00	0.74	0.62
	9	6.04	0.17	11.12	8.38	0.25	0.19	0.00	0.75	0.57
	10	5.13	0.15	10.67	8.08	0.20	0.14	0.00	0.76	0.50
	11	7.07	0.20	10.74	8.43	0.24	0.07	0.00	0.78	0.68
	12	5.54	0.21	9.06	6.92	0.22	0.10	0.00	0.76	0.64
	13	5.87	0.11	9.39	7.33	0.25	0.15	0.00	0.78	0.65
	14	6.64	0.34	10.46	8.20	0.36	0.11	0.00	0.78	0.67
	15	6.73	0.25	10.89	8.55	0.27	0.12	0.00	0.79	0.64
	16	5.61	0.17	10.02	7.46	0.22	0.13	0.00	0.74	0.58
	17	5.05	0.12	9.62	8.37	0.36	0.08	0.00	0.87	0.56
	18	6.30	0.26	9.96	8.02	0.23	0.15	0.00	0.81	0.66
	19	5.59	0.34	10.38	8.77	0.40	0.20	0.00	0.84	0.58
	20	5.52	0.11	10.67	8.10	0.24	0.17	0.00	0.76	0.54
	21	5.71	0.08	10.55	7.55	0.18	0.16	0.00	0.72	0.56
	22	5.51	0.27	11.01	7.83	0.30	0.12	0.00	0.71	0.53
	23	4.83	0.31	9.92	10.64	0.50	0.29	0.00	1.07	0.54
	24	4.87	0.25	11.12	11.94	0.78	0.35	0.00	1.07	0.51
	25	4.81	0.49	10.11	10.38	0.62	0.23	0.00	1.03	0.54
	26	4.21	0.30	8.76	8.72	0.47	0.15	0.00	1.00	0.53
	27	5.83	0.13	11.62	8.28	0.28	0.11	0.00	0.71	0.53
	28	5.90	0.43	10.18	9.06	0.36	0.18	0.00	0.89	0.61
	29	4.94	0.33	10.44	8.52	0.27	0.17	0.00	0.82	0.50
	30	4.81	0.50	10.08	9.23	0.34	0.30	0.00	0.92	0.51
L2	31	5.78	0.00	14.06	8.08	0.34	0.00	0.00	0.57	0.44
	32	7.07	0.19	13.59	8.39	0.29	0.12	0.00	0.62	0.54
	33	7.38	0.09	14.13	9.41	0.29	0.15	0.00	0.67	0.54
	34	6.63	0.00	13.57	9.31	0.00	0.00	0.00	0.69	0.49
	35	6.91	0.30	14.54	10.32	0.44	0.11	0.00	0.71	0.51
	36	6.57	0.39	13.32	8.66	0.20	0.08	0.00	0.65	0.51
	37	6.38	0.00	14.01	8.62	0.00	0.00	0.00	0.62	0.46
	38	6.33	0.16	13.34	8.88	0.10	0.16	0.00	0.67	0.48
	39	5.60	0.35	13.22	8.56	0.20	0.38	0.00	0.65	0.44
	40	6.40	0.12	12.58	8.66	0.26	0.17	0.00	0.69	0.53
	41	6.20	0.30	12.91	8.97	0.25	0.12	0.00	0.69	0.50
Average		6	0.2	11	9	0.3	0.2	0.00	0.8	0.6
2 × stdev		1	0.3	3	2	0.3	0.2	0.00	0.2	0.1

L1 = Location 1 and L2 = Location 2 in Fig. 7; stdev = standard deviation.

Table 5
Chemical compositions (at.%) of geopolymer phase in Na-FAC1 sample.

Position	Na	Mg	Al	Si	K	Ca	Fe	Si/Al	(K + Na)/Al
1	10.76	0.00	13.05	13.15	0.32	0.00	0.00	1.01	0.85
2	10.19	0.00	12.75	13.26	0.36	0.00	0.00	1.04	0.83
3	9.13	0.00	12.04	12.45	0.35	0.00	0.00	1.03	0.79
4	10.07	0.00	12.98	13.55	0.52	0.00	0.00	1.04	0.82
5	9.73	0.00	12.97	13.67	0.52	0.00	0.00	1.05	0.79
6	9.44	0.00	12.29	13.02	0.38	0.00	0.00	1.06	0.80
7	10.16	0.00	12.50	12.79	0.36	0.00	0.00	1.02	0.84
8	10.15	0.00	11.25	11.65	0.41	0.50	0.00	1.04	0.94
9	9.04	0.00	11.10	11.54	0.31	0.00	0.00	1.04	0.84
10	9.85	0.00	12.33	12.79	0.39	0.00	0.00	1.04	0.83
11	9.33	0.00	12.18	12.49	0.35	0.00	0.00	1.03	0.79
Average	10	0.00	12	13	0.4	0.1	0.00	1.04	0.83
2 × stdev	1	0.00	1	1	0.1	0.3	0.00	0.03	0.09

stdev = standard deviation.

Table 6
Chemical compositions (at.%) of probable C–S–H(I) phase in Na-FAC1 sample.

Position	Na	Mg	Al	Si	K	Ca	Fe	Ca/Si	Ca/Mg	Approximate Al/Si in CSH(I)
C1	0.00	4.05	5.65	12.45	0.00	9.23	1.66	0.74	2.28	0.33
C2	0.00	4.18	4.49	13.27	0.00	9.46	1.57	0.71	2.26	0.21
C3	0.00	3.17	6.82	11.70	0.00	9.01	1.89	0.77	2.84	0.48
C4	0.00	3.95	5.45	13.05	0.00	9.61	1.89	0.74	2.43	0.30
C5	0.00	4.02	4.86	13.28	0.00	9.52	1.61	0.72	2.37	0.25
C6	0.00	4.23	4.59	13.23	0.00	9.51	1.49	0.72	2.25	0.22
C7	0.70	3.40	5.70	11.32	0.00	8.82	1.69	0.78	2.59	0.39
C8	0.00	3.84	5.40	12.63	0.00	9.26	1.45	0.73	2.41	0.31
C9	0.62	3.86	5.60	13.61	0.00	10.23	1.64	0.75	2.65	0.30
C10	0.57	3.98	4.79	13.10	0.00	9.59	2.33	0.73	2.41	0.25
Average	0.2	3.9	5	13	0.00	9.4	1.7	0.74	2.5	0.3
2 × stdev	0.6	0.7	1	1	0.00	0.8	0.5	0.04	0.4	0.2

stdev = standard deviation.

Table 7
Chemical compositions (at.%) of geopolymer phase in FAC2 sample.

Location	Position	Na	Mg	Al	Si	S	K	Ca	Fe	Si/Al	(K + Na)/Al
L1	1	6.41	0.75	10.85	9.85	0.75	0.27	0.42	0.00	0.91	0.62
	2	6.45	0.60	8.26	8.69	0.72	0.25	0.22	0.00	1.05	0.81
	3	5.49	0.36	6.74	6.70	0.61	0.25	0.00	0.00	0.99	0.85
	4	8.24	0.34	8.93	9.46	0.92	0.31	0.21	0.00	1.06	0.96
	5	8.66	0.54	8.84	9.99	1.09	0.34	0.00	0.00	1.13	1.02
	6	8.25	0.52	7.92	9.86	0.89	0.24	0.00	0.00	1.24	1.07
	7	8.91	0.42	8.45	9.61	0.94	0.26	0.25	0.00	1.14	1.09
	8	6.46	0.72	9.62	9.47	0.59	0.26	0.37	0.52	0.98	0.70
	9	8.66	0.61	7.55	9.22	0.85	0.22	0.25	0.00	1.22	1.18
	10	7.44	1.29	7.68	9.80	0.61	0.30	0.50	0.57	1.28	1.01
	11	7.90	0.73	9.07	10.27	0.72	0.00	0.37	0.51	1.13	0.87
L2	12	5.19	0.89	9.32	7.07	0.51	0.30	0.00	0.70	0.76	0.59
	13	6.51	0.55	9.59	7.81	0.77	0.00	0.00	0.41	0.81	0.68
	14	5.73	0.00	8.20	9.46	0.81	0.00	0.24	0.00	1.15	0.70
	15	5.84	0.00	11.97	8.33	0.00	0.00	0.00	0.00	0.70	0.49
	16	4.79	0.83	11.21	7.58	0.53	0.27	0.00	0.63	0.68	0.45
	17	5.73	0.00	8.20	8.08	0.00	0.00	0.00	0.00	0.99	0.70
	18	7.15	0.00	10.23	9.43	0.79	0.27	0.35	0.00	0.92	0.73
	19	4.85	0.66	10.74	7.55	0.51	0.29	0.26	0.00	0.70	0.48
	20	5.43	0.00	7.77	9.79	0.71	0.40	0.00	0.00	1.26	0.75
	21	6.71	0.63	10.63	7.78	0.00	0.31	0.00	0.00	0.73	0.66
	22	7.32	0.61	8.94	9.13	1.03	0.48	0.29	0.00	1.02	0.87
Average		7	0.5	9	9	0.7	0.2	0.2	0.2	1.0	0.8
2 × stdev		3	0.7	3	2	0.6	0.3	0.3	0.5	0.4	0.4

L1 = Location 1 and L2 = Location 2 in Fig. 9; stdev = standard deviation.

Table 8
Chemical compositions (at.%) of geopolymer phase in Na-FAC2 sample.

Position	Na	Mg	Al	Si	S	K	Ca	Fe	Si/Al	(K + Na)/Al
1	9.49	0.46	9.34	9.90	0.00	0.00	0.49	0.00	1.06	1.02
2	9.69	0.45	8.58	9.30	0.72	0.20	0.00	0.00	1.08	1.15
3	9.39	0.00	8.90	8.59	0.82	0.00	0.95	0.00	0.97	1.06
4	9.41	0.84	9.21	9.29	0.63	0.00	0.30	0.00	1.01	1.02
5	9.13	0.27	8.25	9.37	0.65	0.21	0.36	0.00	1.14	1.13
6	10.22	0.46	8.91	9.45	0.00	0.28	0.37	0.00	1.06	1.18
7	8.81	0.84	10.33	8.97	0.80	0.26	0.20	0.00	0.87	0.88
8	9.55	0.73	7.78	9.95	0.00	0.32	0.94	0.00	1.28	1.27
9	8.01	0.00	10.92	12.63	0.81	0.31	0.89	0.00	1.16	0.76
10	10.28	0.46	11.97	12.03	1.12	0.00	0.74	0.00	1.01	0.86
11	7.99	0.77	9.40	9.01	1.01	0.31	1.09	0.00	0.96	0.88
12	9.31	0.72	10.73	10.30	0.00	0.33	1.59	0.00	0.96	0.90
13	9.23	0.66	6.36	9.59	0.00	0.00	1.54	0.00	1.51	1.45
Average	9	0.5	9	10	0.5	0.2	1	0.00	1.0	1.0
2 × stdev	1	0.6	3	2	0.9	0.3	1	0.00	0.3	0.4

stdev = standard deviation.

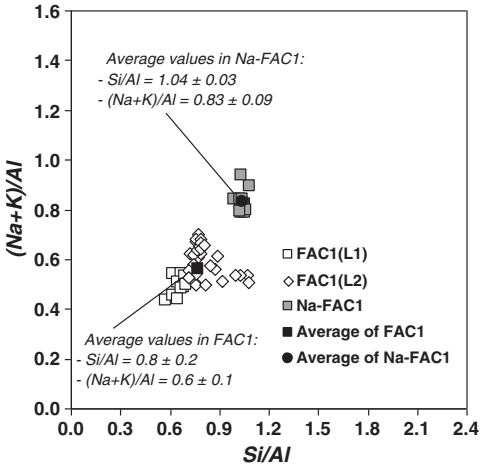

Fig. 11. Plot of atomic ratio of (Na + K)/Al vs. Si/Al for geopolymer phases of FAC1 (see Fig. 7) and Na-FAC1 (see Fig. 8). Note: L1 = Location 1 and L2 = Location 2 in Fig. 7.

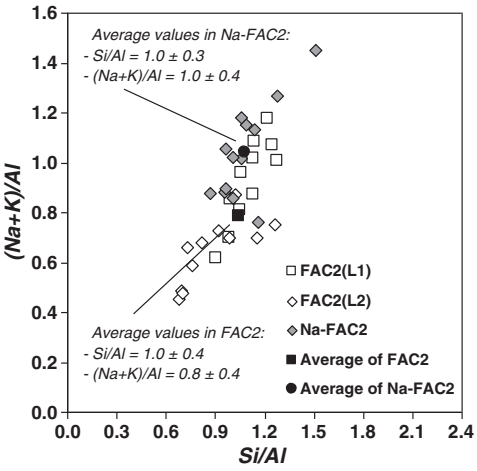

Fig. 12. Plot of atomic ratio of (Na + K)/Al vs. Si/Al for geopolymer phases of FAC2 (see Fig. 9) and Na-FAC2 (see Fig. 10). Note: L1 = Location 1 and L2 = Location 2.

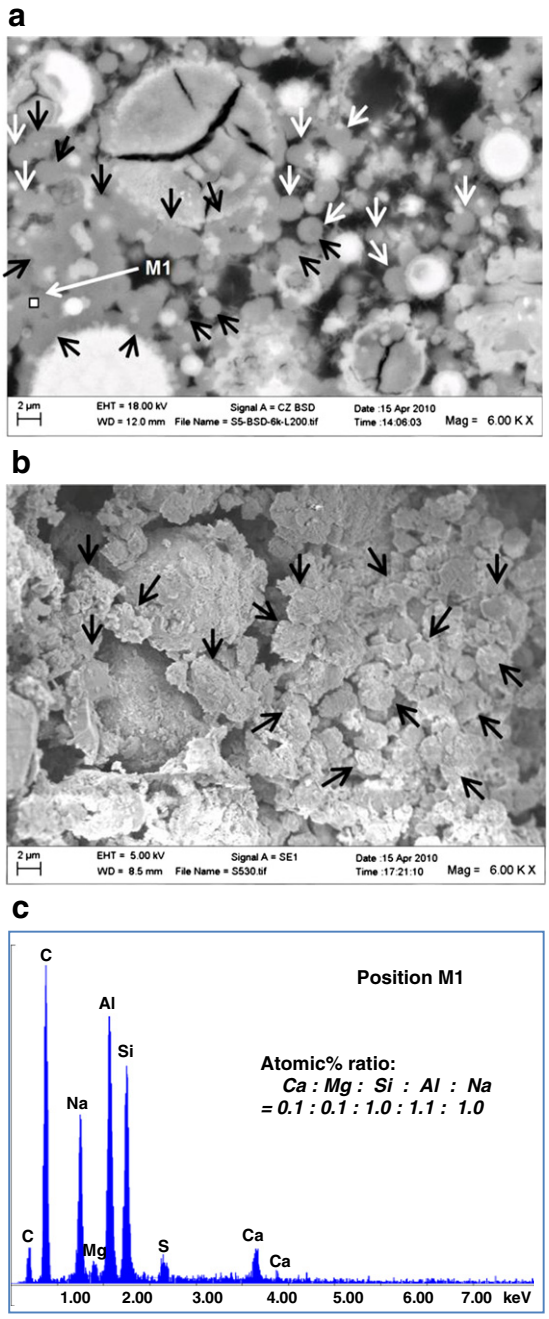

Fig. 13. Particulate geopolymeric products of activated Na-FAC2 in (a) BSE image from carbon-coated sample for the area marked by Z in Fig. 10; (b) SE image of a pore area from gold-coated sample; both white and black arrows designate the geopolymeric products and (c) spot analysis chemical composition of position M1 shown in (a).

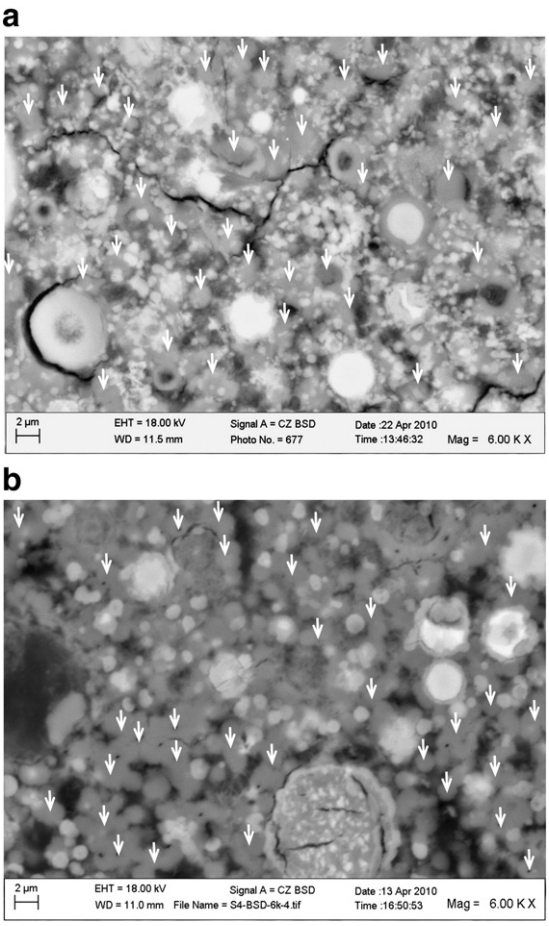

Fig. 14. Indicated with white arrows, dark grains with a few hundred nanometer sizes up to ~2 μm are geopolymers, (bright particles possibly indicate C–S–H(I) particles): (a) a BSE image of FAC1 for the area marked by box X in Fig. 7; and (b): a BSE image of Na-FAC1for the area marked by box Y in Fig. 8.

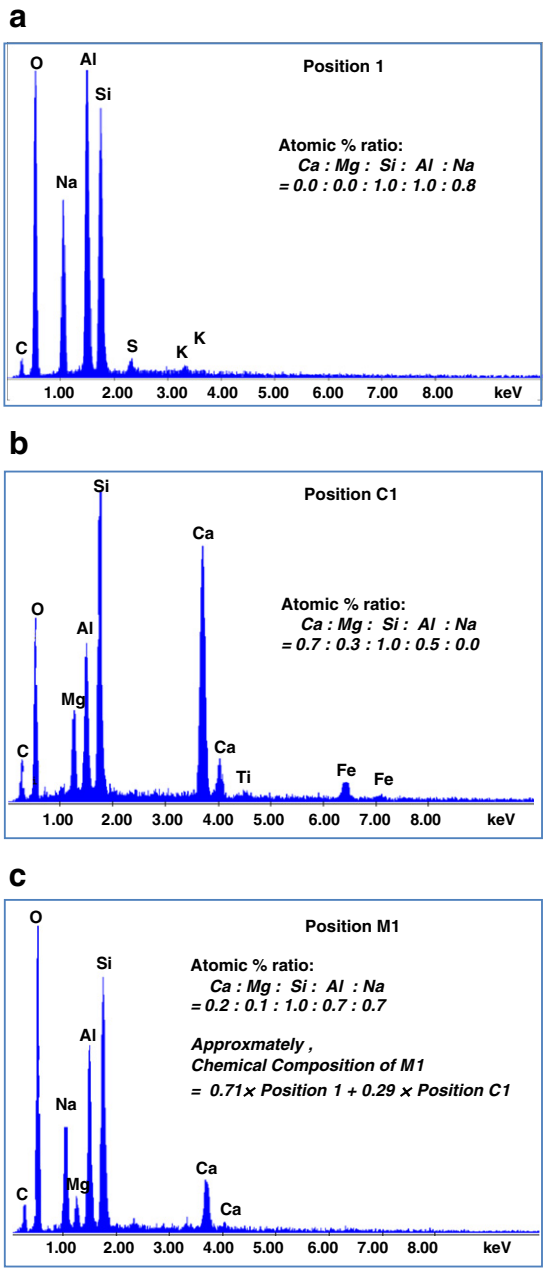

Fig. 15. Chemical spot analysis for the locations shown in Fig. 8 (see 1, C1 and M1 in the figure): (a) represents geopolymer phase; (b) represents C–S–H(I) phase; and (c) indicates a mixture of geopolymer and C–S–H(I) phases with respect to chemical composition.